STOMATIN-LIKE PROTEIN 2 LINKS MITOCHONDRIA TO T CELL RECEPTOR SIGNALOSOMES AT THE IMMUNOLOGICAL SYNAPSE AND ENHANCES T CELL ACTIVATION

By

Mark G Kirchhof[1], Luan A. Chau[1], Caitlin D. Lemke[1], Santosh Vardhana[2], Peter J. Darlington[1, *], Maria E. Márquez[3], Roy Taylor[4], Kamilia Rizkalla[4], Isaac Blanca[3], Michael L. Dustin[2], and Joaquín Madrenas[1, **]

from

[1]The FOCIS Centre for Clinical Immunology and Immunotherapeutics, Robarts Research Institute, and the Departments of Microbiology and Immunology, and Medicine, the University of Western Ontario, London ON, Canada N6A 5K8; [2]Program in Molecular Pathogenesis, Skirball Institute of Biomolecular Medicine, New York, NY 10021, USA; [3]Instituto de Inmunologia, Universidad Central de Venezuela, Caracas, Venezuela; and [4]Department of Pathology, London Health Sciences Centre, London, ON, Canada N6A 5K8.

[*]Current address: Montreal Neurological Institute and Hospital, Room W010, 3801 University St., Montreal, Quebec, H3A 2B4

[**]Address correspondence and reprint requests to J. Madrenas, at Robarts Research Institute, Room 2.05, P.O. Box 5015, 100 Perth Drive, London, Ontario, Canada N6A 5K8, e-mail: madrenas@robarts.ca, FAX: (519) 663-3443.

Summary

T cell activation through the antigen receptor (TCR) requires sustained signalling from microclusters in the peripheral region of the immunological synapse (IS). The bioenergetics of such prolonged signaling have been linked to the redistribution of mitochondria to the IS. Here, we report that stomatin-like protein-2 (SLP-2) plays an important role in this process by bridging polarized mitochondria to these signaling TCR microclusters or signalosomes in the IS in a polymerized actin-dependent manner. In this way, SLP-2 helps to sustain TCR-dependent signalling and enhances T cell activation.

Introduction

$CD4^+$ T cell activation involves the formation of a highly organized interface between the T cell and the antigen-presenting cell (APC) known as the IS [1-4]. This process requires selective polarization of some surface and intracellular molecules to the IS-proximal pole [5] and of others to the antipodal pole of the T cell [6,7], in a cytoskeleton-dependent manner. Furthermore, T cell polarization is highly dynamic as illustrated, within the IS, by the early detection of signalling microclusters in the outer ring of the synapse [8] and their subsequent movement, as activation proceeds, to the centre of the synapse where they are internalized and destined to degradation [2,3,9] to ensure signal down-regulation [10].

A picture on how TCR signalling orchestrates cytoskeletal reorganization and polarization of surface and intracellular molecules is rapidly emerging [11-13]. However, much less is known about translocation and anchoring of organelles during T cell polarization. Recently, two reports have nicely documented the redistribution of mitochondria during different states of T cell function. Specifically, mitochondria translocate to the IS during T cell activation [14], but relocate to the uropod during T cell locomotion [15]. Such a dynamic partitioning of mitochondria may have important implications in assuring the bioenergetics required for sustained signaling which in turn is required for full T cell responses.

To identify novel components of the molecular machinery that "bridge" TCR signalosomes with the cytoskeleton and cellular organelles, we performed a proteomic analysis of lipid raft microdomains from T cells undergoing activation through their TCR. Such an approach identified stomatin-like protein 2 (SLP-2) (also known as STOML2 or EPB72), a finding corroborated by other groups [16,17]. SLP-2 is a member of the highly conserved stomatin family of proteins whose homologs span from archae to humans and include stomatin, SLP-1,

and SLP-3 [18-22]. SLP-2 shares a central SPFH (stomatin/prohibitin/flotillins/HflK-HflC) domain characteristic of this family that may mediate interactions with membrane proteins [23-25]. However, SLP-2 is unique among stomatins in that it does not have a putative transmembrane domain, but has six myristoylation/palmitoylation sites and an N terminal mitochondria targeting sequence [25,26].

The function of stomatins, including SLP-2, is unknown. It has been suggested that they are involved in the organization of the peripheral cytoskeleton, and in the assembly of ion channels [25,27-30] and mechanosensation receptors [31-37]. Here, we report that SLP-2 provides a structural link between synapse-polarized mitochondria and TCR signalosomes, and thus contributes to modulate TCR signaling and T cell activation.

Results

To explore the involvement of SLP-2 in immune cell activation, we first looked at its expression within human hematopoietic organs and tissues. We detected SLP-2 mostly in lymph nodes and thymus, and in lower amount, in tonsils (figure 1A). Little expression was detected in spleen and resting peripheral blood leukocytes, and the differences were not due to protein loading as normalized by blotting with glyceraldehyde-3-phosphate dehydrogenase (GAPDH). In individuals in which SLP-2 was detectable in peripheral blood mononuclear cells, it was expressed by monocytes, and to less extent, by T and B lymphocytes (supplemental figure 1).

In lymph nodes, SLP-2 was mostly detected in the paracortical (T cell) area and in the germinal centres (B cell area) (figure 1B). In the thymus, SLP-2 expression was higher in the cortex than in the medulla (figure 1B). The higher expression of SLP-2 in sites where lymphocyte signaling and activation takes place (i.e., antigen activation in lymph nodes and

tonsils, positive and negative selection in the thymus) prompted us to examine the effect of activation on SLP-2 expression. Although peripheral blood T cells express low levels or no SLP-2 under resting conditions, activation of these cells with bacterial superantigens led to a significant up-regulation of its expression (figure 1C). Similarly, in B cell preparations from human tonsils fractionated according to their activation status, SLP-2 was mostly detected in the fraction corresponding to activated memory ($CD20^{bright}$, $CD27^{+}$) B cells (figure 1D). Seventy three percent of cells in this fraction (f1) were activated memory B cells (as indicated by expression of CD27), and only 8% of cells in this fraction were naïve B cells. In contrast, 60% of the cells in fraction 4 were naïve B cells and only 11% were activated memory B cells. Fractions 2 and 3 had progressively decreasing numbers of activated memory B cells (52% and 32%, respectively) and increasing numbers of naïve B cells (17% and 45% respectively). Therefore, the profile of SLP-2 expression in these fractions correlated with the presence of activated memory B cells. Together these data led us to conclude that SLP-2 expression is up-regulated by *in vivo* and *ex vivo* lymphocyte activation.

To define the role of SLP-2 in T cell activation, we next established its intracellular distribution in resting T cells and during activation with APC and the staphylococcal enterotoxin E (SEE) bacterial superantigen. In Jurkat T cells stably transfected with a doxycycline-inducible, green fluorescence protein (gfp)-tagged SLP-2 (SLP-2-gfp), we identified two pools of SLP-2. Most SLP-2 signal was detected in intracellular clusters distributed in a relatively even fashion throughout the cell. In addition, a second small but significant pool of SLP-2 was consistently detected in the periphery of the cytoplasm and appeared to be associated with the inner leaflet of the plasma membrane (figure 2A). Similar distribution was observed with indirect immunofluorescence of endogenous SLP-2 using an antiserum against SLP-2

(supplemental figure 2). The presence of two pools of SLP-2 within T cells was also documented by immunoblotting of subcellular T cell fractions (supplemental figure 3).

Upon activation of these Jurkat T cells with APC and SEE, both pools of SLP-2 (plasma membrane-associated pool and intracellular pool) converged towards putative synapses, and coalesced into a major cluster close to the plasma membrane in the periphery of the IS and underneath the T cell-APC interface (figure 2B). Such a polarization of SLP-2 was observed in more than 60% of T cells and was not due to "nuclear exclusion" or non-specific redistribution of molecules to the IS as we [7] and others [6,38] have shown for gfp-tagged signaling molecules (e.g., phosphodiesterase 4B2). Next, we examined the redistribution of SLP-2 once it had relocated to the IS. We found that, after polarizing to the T cell:APC interface, more than 80% of the polarized SLP-2-gfp partitioned in the periphery of the synapse and underneath the IS as activation proceeded, and only a small fraction of SLP-2 was detectable in the centre of the IS where downregulated TCR clusters are (figure 2C and supplementary video 1).

The polarization of SLP-2 during T cell activation was examined in more detail using supported planar bilayers containing anti-CD3 and ICAM-1 to which T cells form IS-like structures (figure 3 and supplementary videos 2A and 2B). This system has excellent optics for resolution of components in the IS. With this system, and under conditions of doxycycline-induced SLP-2-gfp overexpression, we confirmed the presence of two pools of SLP-2. The plasma membrane-associated pool of SLP-2 was visualized by total internal reflection fluorescence microscopy (TIRFM) as weak but consistent signal clusters located at less than 200nm from the glass plane (i.e., sites of TCR and LFA-1 engagement) (figure 3A). In the early or nascent IS, this pool of SLP-2 was distributed in a uniform granular appearance with TCR microclusters (figure 3A top row). However, as activation proceeded, we observed a reduction

of SLP-2 fluorescence in the TCR microclusters as these relocated to the centre of the IS (up to 50% reduction) (figure 3A bottom row), while densely packed SLP-2 clusters were still observed in the periphery of the IS. It is important to note that the TCR clusters at the centre of the synapse have been identified as not-signaling clusters any more but as TCR oligomers destined to internalization and degradation.

The major pool of SLP-2-gfp, located at more than 200 nm from the plasma membrane, also polarized to the IS and distributed close to the pSMACs, segregated from the cSMACs, as activation proceeded (figure 3B, supplementary video 2A, and Table 1). This major pool of SLP-2 within the cell was identified as associated with mitochondria as shown by the co-localization of the gfp signal with a mitochondria-targeted red fluorescence protein (mtRFP) (figure 3C). Of interest, such a polarization of mitochondria to the IS has been recently confirmed by another group [14].

The polarization of SLP-2 to the IS and its peripheral distribution once in the synapse required TCR engagement because, as determined by wide field fluorescence microscopy, it was observed in 100% of the cells forming an IS in response to TCR/LFA-1 co-ligation but in none of the cells responding to LFA-1 ligation alone (Table 2, and supplementary videos 2A and 2B).

The distribution of SLP-2 during T cell activation was stable as shown by fluorescence recovery after photobleaching (FRAP) (figure 4 and supplementary videos 3A and 3B). In these experiments, the SLP-2 signal was restored after 400 seconds of bleaching the plasma membrane of non-stimulated T cells but was not restored when SLP-2-gfp clusters in OKT3-stimulated T cells were bleached within the same timeline. Furthermore, we documented that SLP-2 was detected in lipid rafts and its partitioning to these microdomains increased during T cell activation (supplemental figure 4).

The dynamic redistribution of both pools of SLP-2 to the IS suggested the idea that they participate in signalling from the TCR. So, we tested if SLP-2 interacted with the components of TCR signalosomes during activation for up to 60 minutes, a time window that covers the formation of signalling microclusters and mature IS (figure 5A). We observed that SLP-2 steadily associated with the CD3 ε chain of the TCR complex under resting conditions and during the 60 minutes of stimulation. With co-precipitation studies, we determined that about 0.09% of the cellular SLP-2 associated with the TCR complex (supplemental figure 5). The association of SLP-2 with the TCR/CD3 complex was selective because no association of SLP-2 with other surface receptors (e.g., CD45, CTLA-4) or with control intracellular molecules (RasGAP, caspase 3 – see below) was detected (figure 5A and data not shown). Furthermore, the interaction of SLP-2 with cell surface receptors was documented by co-precipitation of SLP-2-gfp with biotinylated surface receptors and was lost when SLP-2-gfp lacked the N terminal membrane-targeting signal of SLP-2 (supplemental figure 6).

SLP-2 interacted with Lck under basal conditions, and this interaction increased for up to 15 minutes of stimulation, beyond which it decreased and disappeared by 60 minutes of stimulation. The pool of Lck associated with SLP-2 included both active Lck and recently activated Lck as illustrated by the detection of p56 and p59 Lck forms. SLP-2 also associated with ZAP-70 but the association with this kinase occurred after 1 minute of stimulation and lasted for only 5 minutes, decreasing afterwards to practically undetectable levels (figure 5A). The profile of SLP-2 association with ZAP-70 during TCR signaling is consistent with the findings of other co-precipitation studies [39] and compatible with the sequential involvement of Lck and ZAP-70 in early TCR signalling [40]. We also documented the interaction of SLP-2 with LAT, and of SLP-2 with the active (phosphorylated) form of PLC-γ1 between 1 peaking at 5

minutes of stimulation and decreasing afterwards. Of interest, we observed the association between SLP-2 and non-phosphorylated PLC-γ1 during the full time course (figure 5A), suggesting that SLP-2/PLC-γ1 complexes may be preassembled before TCR signalling.

During synapse formation, LFA-1 is organized in microclusters in the pSMAC. In this area, LFA-1 microclusters are interspersed with TCR microclusters [9]. As predicted by the location of SLP-2 in the periphery of the IS, we found that, upon activation with SEE and APC, there was a rapid increase in the level of association of SLP-2 with LFA-1 that decreased at later time points of activation (figure 5B).

It is important to note that all the co-precipitation studies reported above were performed under high stringency condition with strong detergents (Triton X-100 1%). Also, under these conditions, we detected selective interactions of SLP-2 with only some receptors and signaling molecules but not with other molecules (e.g., CD45, CTLA-4, RasGAP, caspase 3).

Since TCR signaling leads to cytoskeletal reorganization, and since the cytoskeleton is required for intracellular movement of mitochondria, we predicted that the association of SLP-2 with the TCR signalosome and with mitochondria during T cell activation would involve the cytoskeleton. To test this idea, we examined the interaction of SLP-2 with actin. We found that SLP-2 interacted with actin under resting conditions and upon TCR stimulation (figure 5C). SLP-2 also interacted with vav, a small GTPase that regulates cytoskeletal reorganization, and with Nck, an adaptor protein that links transmembrane and scaffolding molecules to the cytoskeleton [41] (and this interaction peaked at the times of maximal interaction between SLP-2 and the components of the signalosome) (figure 5C). The association between SLP-2 and cytoskeletal molecules was not observed using a control pre-immune serum, ruling out a non-specific association. Furthermore, the association between SLP-2 and β-actin during T cell

activation involved the polymerized form of actin because cytochalasin D, an inhibitor of actin polymerization, completely prevented this interaction (figure 5D). It is important to note that T cell activation in our system is dependent on actin polymerization, because inhibition of actin polymerization led to inhibition of IL-2 production (figure 5D).

Next, we examined the biological implications of the interactions between SLP-2 and the components of the TCR signalosome. We reasoned that, if SLP-2 was required for signaling from the TCR signalosomes, then knocking down SLP-2 would decrease TCR signalling. To test this hypothesis, we knocked down SLP-2 expression by RNA interference using two different sets of siRNAs. We found that the effect of SLP-2 down-regulation on IS formation was minimal (although statistically significant over multiple experiments) (figure 6A; this figure shows one example of synapse-forming, SLP2 siRNA-treated T cell – panel #1 - and one example in which no synapse was observed – panel #2). However, as predicted, SLP-2 down-regulation significantly shorten the timeline of TCR signaling (Figure 6B). We found that, at equal levels of early TCR signaling (as measured by similar levels of initial ERK-1/-2 activation), down-regulation of SLP-2 caused a remarkably shorter duration of ERK activation in response to TCR stimulation, already apparent at 5 minutes and still significant at 10 minutes of stimulation (figure 6B).

The effect of SLP-2 down-regulation on TCR signalling was functionally significant. Using Jurkat T cells stably transfected with a doxycycline-inducible SLP-2-gfp, we found that *de novo* over-expression of SLP-2 (as corroborated by FACS) significantly increased IL-2 production in response to SEE and APC (figure 7A). In contrast, knocking-down the expression of SLP-2 in Jurkat T cells (by about 80% on average, with three different siRNA constructs) correlated with a significant decrease of the IL-2 response to APC and SEE (figure 7A). These

findings were corroborated with primary human T lymphocytes from normal volunteers. Naïve T cells express low levels of SLP-2 (figure 7B). However, upon activation, SLP-2 protein expression is up-regulated significantly within 30-42 hours. Thus, to induce high expression of SLP-2 in primary human T lymphocytes, we pre-activated these cells with a mitogenic combination of phorbol ester and ionomycin for 3 days, followed by a resting period. At this point, these effector T cells and their naïve T cell counterparts from the same donor were nucleofected with SLP-2 siRNA or control siRNA, re-stimulated with SEE and APC for 24 hours, and their IL-2 response examined. As shown in figure 7B, knocking-down the expression of SLP-2 by more than 60% correlated with a significant decrease in the IL-2 response of the effector T cells (around 10-100 times) as illustrated by the 'shift to the right' of the dose-response curve to SEE ($p<0.001$). Little effect was observed for SLP-2 siRNA in resting T cells in which SLP-2 expression is almost absent. Also, SLP-2 siRNA had no effect on the IL-2 response of human T cells to mitogenic stimulation with PMA and ionomnycin, which bypasses membrane-associated events (supplemental figure 7). Therefore, we concluded that down-regulation of SLP-2 expression prevented sustained TCR signaling and decreased IL-2 production by effector T cells.

Discussion

To our knowledge, we provide the first biological evidence of a function for SLP-2 in an eukaryotic cell type - that of sustaining TCR signalling and enhancing T cell activation. Such a role involves the redistribution of two subcellular pools of SLP-2, one in association with mitochondria and the other with the plasma membrane, and their convergence at the IS. Under resting conditions, SLP-2 is mostly located in mitochondria and, less abundantly, in association

with the plasma membrane. Upon T cell activation, both pools of SLP-2 converge and coalesce into the peripheral area of the IS, a region where signaling TCR microclusters have been reported to accumulate [9]. At the biochemical level, the redistribution of SLP-2 correlates with SLP-2 interaction with components of the TCR signalosomes and with polymerized actin. At the functional level, such a redistribution correlates with modulation of SLP-2 expression regulating the profile of TCR signaling and the magnitude of T cell responses. Putting these observations together, we suggest that SLP-2 contributes to sustain TCR signalling and enhances T cell activation by bridging mitochondria to TCR signalosomes through polymerized actin, ensuring the bioenergetic requirements of TCR-dependent signalling.

Using morphological and biochemical approaches, we have identified two pools of SLP-2 in T cells: a plasma membrane-associated one and a mitochondrial one. Such a profile of intracellular distribution is in line with the presence of myristoylation-palmitoylation sites in SLP-2 as well as by a good mitochondria-targeting sequence in its N terminus [25], and it is consistent with the detection of SLP-2 in membranes of other cell lineages [16,42-44]. Of interest, the presence of SLP-2 in mitochondria and plasma membrane is also reminiscent of the finding of other proteins (e.g., porin) in both pools [45].

Our findings identify a novel regulatory mechanism of TCR signaling based on cytoskeleton-dependent interaction between signaling TCR microclusters or signalosomes and cellular organelles [12]. Such a mechanism may be applicable to other members of the lipid raft–enriched, prohibitin-flotillin-stomatin family of proteins [46,47]. For example, prohibitin is indispensable for the activation of the Ras-ERK signalling pathway [48], a role also proposed for the flotillins [49-51]. Although the interaction of plasma membrane SLP-2 with the TCR signalosome components during activation was too small to be visualized by current imaging

techniques, it was clearly documented by the biochemical studies. Also, the visualization of SLP-2 exclusion from TCR clusters at the centre of the synapse at late timer points of activation is consistent with our interpretation of SLP-2 interaction with the signaling TCR clusters, as the TCR clusters at the centre of the synapse are not signaling but destined to degradation. In addition, the imaging studies demonstrated that both pools of SLP-2 coalesce and stably position close to the peripheral areas of the synapse.

The redistribution of the mitochondrial pool of SLP-2 to the IS is consistent with the recently reported translocation of these organelles to the IS [14]. Such mitochondrial partitioning is one more example of an emerging broader concept of translocation of these organelles to different poles of the cell during biological responses, through nitochondrial fission and fusion and in a cytoskeleton and/or microtubule-dependent fashion [52] . For example, mitochondria relocate to the uropod during T cell locomotion through a mechanism that involves microtubules and mitochondrial fission [15]. In contrast to locomotion, we would suggest that the relocation of SLP-2 to the IS during T cell activation reflects net mitochondrial fusion. Such a possibility is suggested by the recent report that mitofusin-2, a mitochondrial fusion protein, can interact with SLP-2 in vitro [25], and by preliminary data indicating that overexpression of SLP-2 up-regulates the expression of proteins involved in mitochondrial fusion (C.D.L and J.M., unpublished observations). The precise structural complex that bridges the mitochondria with the cytoskeleton through SLP-2 is still unknown.

Finally, we show that modulation of SLP-2 expression regulates T cell activation, so that increasing the levels of SLP-2 enhances IL-2 responses while decreasing SLP-2 expression decreases Il-2 responses. It is important to note that, as we show, up-regulation of SLP-2 expression occurs *in vivo* and *ex vivo* during lymphocyte activation. Such a finding may partially

explain the long-standing observations that, at equal requirement for sustained signaling, primary naïve T cells show much fainter signal transduction than primed T cells and that the responsiveness of primed T cells is greater than that of naïve T cells. Most studies of TCR microclusters and IS formation have also used effector T cells, which require fewer engaged TCRs as well as less CD28-dependent costimulation. One may therefore argue that the up-regulation of SLP-2 may be one of the factors that contribute to enhance the responsiveness of effector lymphocytes by providing more effective sustained signaling from TCR signalosomes [53,54].

Material and methods

Plasmids, siRNA and T cell transfectants. Human SLP-2 cDNA was subcloned into the pEGFP-N1 expression vector (Clontech Inc. Palo Alto, CA) to create an in-frame translational fusion of SLP-2 and gfp at the 3' end. Subsequently, the SLP-2-gfp was placed into the doxycycline-inducible pBig2i vector [55]. Stable transfectants were generated by electroporating linearized plasmid into Jurkat E6.1 T cells and screened for stable expression. Doxycycline (Sigma, St. Louis, MO) was added in culture overnight at 1000 ng/mL to induce SLP-2-gfp expression. Expression of SLP-2-gfp was monitored by direct flow cytometry (Becton Dickinson, CA). RNA interference targeting SLP-2 (cat # 20643 and 20467) was obtained (Ambion, Austin, TX) and transfected into Jurkat T cells or PBMC and PBMC blasts using either the Nucleofector kit for cell lines or for human primary T cells (Amaxa, Gaithersberg, MD). As controls for SLP-2 siRNA, we used negative control siRNAs provided by the commercial supplier (Ambion). These controls siRNAs have no significant similarity to any known gene sequences from mouse, rat, or human and no toxicity to cells, have been shown to lack any significant effect in cell

proliferation and apoptosis assays, and do not modulate the mRNA levels of "housekeeping" genes (18S rRNA, GAPDH, and cyclophilin) up to 48 hr after transfection. In addition, GFP cDNA was used as a control for nucleofection efficiency. After siRNA or control transfection, cells were rested for 24 hours until optimum down-regulation of SLP-2 was observed before proceeding with any functional assays. The cDNA coding for mitocondria-targeted RFP has been previously described [15] and was kindly provided by Dr. A. Viola (Venetian Institute of Molecular Medicine, Padua, Italy).

Cells. Peripheral blood mononuclear cells (PBMC) were isolated from heparinized whole blood of normal donors using Ficoll-Hypaque (Amersham Pharmacia Biotech, Uppsala, Sweden) gradients. Cells were washed in supplemented RPMI 1640 media and resuspended at 1 x 10^6 cells/ml. PBMC blasts were generated by culturing PBMC with Phorbol Myristate Acetate (PMA; 1 ng/ml) and Ionomycin (100 ng/ml) for 72 hours at 37^{o}C, 5 % CO_2. T cells blasts were rested 48 hours before use in any experiments. Primary T cells were isolated from PBMC using a Pan T cell Isolation Kit (Miltenyi Biotech, Auburn, CA). Jurkat T cells (E6.1) were obtained from American Type Culture Collection (Manassas, VA) and cultured in supplemented RPMI 1640 medium. The B lymphoblastoid cell line LG2, used as APC in some of these experiments, was kindly provided by Dr. Eric Long (NIAID, NIH, Rockville, MD) and cultured in standard supplemented RPMI 1640 media. Lysates from human tissues were obtained from ProSci Inc. (Poway, CA).

Antibodies. An antiserum against human SLP-2 was generated by immunization of rabbits with a peptide spanning amino acids 343 to 356 (ProSci Inc., Poway, CA). Commercially available antibodies against SLP-2 were purchased from Protein Tech Group (Chicago, IL). Immunoblotting for ERK-1/2 was done using a rabbit polyclonal immunoaffinity purified

antiserum (Stressgen Biotechnologies, Victoria, BC, Canada). Actin was immunoblotted using an affinity-purified goat polyclonal antiserum (Santa Cruz Biotechnology Inc., Santa Cruz, CA). CD45 was immunoblotted using a mouse monoclonal (clone 69) antibody (BD Biosciences, Mississauga, ON, CA). Lck and Nck were immunoblotted using rabbit antisera (Upstate Biotechnology, Lake Placid, NY). Isotype control immunoprecipitations were performed using pre-immune serum obtained from ProSci. A pre-immunization serum was used as control for rabbit antisera (ProSci Inc., Poway, CA). Immunoprecipitation of SLP-2 was performed with our SLP-2 antibodies (Prosci, Poway, CA). For confocal microscopy a PE-labelled anti-CD3 (UCHT-I) was used.

Sub-Cellular Fractionation, and Raft isolation. Subcellular T cell compartments were obtained using the Compartmental Protein Extraction Kit (Chemicon, Temecula, CA). Lipid rafts were isolated by sucrose gradient ultracentrifugation following lysis with 0.5% Triton-X-100 as described [56]. Lipid rafts were pelleted by centrifugation of the 1mL raft fraction for 1 hour at 14,000 rpm and 4°C, and were resuspended in lysis buffer and sample buffer for biochemical analysis.

Cell lysates preparation. Jurkat T cells were stimulated with superantigens at final concentration of 1ug/ml, at 37ºC, for 1, 5, 15, 30 and 60 min. Cells were pelleted in PBS containing sodium o-vanadate (400uM) and EDTA (400uM) and lysed in lysis buffer (1% Triton X-100, 150mM NaCl, 10mM Tris (pH7.6), 5mM EDTA, 1mM sodium o-vanadate, 10ug/ml leupeptin, 10ug/ml aprotinin, 25uM p-nitrophenyl-p'-guanidinobenzoate) at 4ºC for 30min. Lysates were cleared of debris (14,000rpm, 4ºC, 10min) followed by immunoprecipitation of target molecules using Ab-coated protein A or G agarose beads.

Cross-linked immunoprecipitation. Protein A agarose beads were coated wih appropriate Abs at 4ºC overnight. Beads were washed four times with room-temperature lysis buffer and four times with PBS. Abs were cross-linked to the beads in 1mg/ml of DSP (Pierce) in PBS, at room temperature rotating for 30mins. The cross-linked Ab-beads were neutralized with 1M Tris, pH8.0 at room-temperature for 5mins; washed once with lysis buffer and four times with PBS, and then used for immunoprecipitation. After immunoprecipitation, beads were pelleted and resuspended in sample buffer without β-Mercaptoethanol. Samples were boiled, pelleted, and supernatant collected, run in SDS-PAGE, and immunoblotted with the indicated Abs.

Tonsil B cells. Highly purified human tonsil B cells by RosetteSep B cell enrichment cocktail (StemCell Technologies,Vancouver, BC, Canada) were fractionated by a seven step Percoll gradient. All fractions were phenotyped for naïve B cells (based on expression of IgM and IgD) and memory B cells ($CD20^{bright}$ and $CD27^{+}$). The proportion of naïve resting B cells increases from fraction 1 to 4 (from 11% to 66% on average) while the proportion of memory/activated B cells decreases from fraction 1 to 4 (from 30% to 3% on average). In addition, each fraction was cultured in vitro to determine spontaneous Ig production. Only fractions 1 and 2 were able to spontaneously secrete Ig (data not shown). Whole cell lysates from B cells in each fraction were prepared and immunoblotted with appropriate specific antibody.

Confocal microscopy. Confocal microscopy was performed with a Zeiss LSM 510 microscope. Jurkat T cells ($1x10^6$/ml), were incubated on poly-lysine-coated (0.01%, Sigma) glass bottom microwell dishes (MatTek Corp., MA) for 10 minutes to promote cell adherence at 37ºC. SLP-2-gfp distribution during IS formation was assessed by culturing doxycycline-induced SLP-2-gfp stably transfected T cells with APCs pre-incubated with 1000 ng/ml SEE for either 10 or 30 minutes. Following the allotted time of co-incubation, the T cell-APC conjugates were rapidly

fixed with paraformaldehyde (4% paraformaldehyde) and washed with PBS/1% FCS and stained with PE conjugated anti-CD3 (BD Bioscience, Mississauga, ON,CA) for 30 min. on ice. For experiments using planar membranes, glass-supported dioleoylphosphatidylcholine bilayers incorporating Cy5-ICAM-1 (300 molecules/μm^2) and 0.1% cap-biotin were prepared in a Bioptechs flow cell. Unlabelled Streptavidin (8 μg/mL) and anti-human CD3, OKT3 clone (10 μg/mL), which was conjugated to Cy3, were loaded sequentially in HBS/HSA buffer. Jurkat T cells were suspended in Hepes buffered saline supplemented with 5 mM glucose, 2 mM $MgCl_2$, 1 mM $CaCl_2$, and 1% human serum albumin (HBS/HSA). All wide field microscopy was performed on an automated microscope with a Hamamatsu USA Orca-ER cooled CCD camera. The hardware on the microscope was controlled using IPLAB software (Scanalytics) on a PowerMac G4 Macintosh computer. Images were exposed in wide field for 1-2 s at a resolution of 0.11 μm per pixel using the 60x 1.45 N.A. objective. Interference reflection microscopy (IRM) is based on destructive interference in green light reflected from the bilayer-cell interface leading to a dark area where cells are in close contact with the bilayer. Images were inspected using Metamorph (Molecular Devices).

T cell functional assays. SLP-2-gfp, SLP-2 siRNA or control transfected T cells ($0.2x10^6$ cells/group) were plated in triplicate on 96 well plates with the B lymphoblast LG2 ($0.1x10^6$ cells/group) with SEE in the presence or absence of 1000 ng/mL doxycycline, at 37°C for 24 hours. Supernatants were collected, and measurement of IL-2 by ELISA was performed following manufacturer specifications (BD Biosciences, Mississauga ON, CA).

Histological analysis. Tissues from thymi and lymph nodes were fixed with 10% formalin, embedded in paraffin, and stained with Hematoxylin and Eosin. Immunohistochemical analysis for SLP-2 was performed with an antisera against SLP-2 at 1/1000 dilution following the

streptavidin-biotin peroxidase method. CD5 and CD20 (monoclonal, mouse anti-human antibodies; Dako) stains were also performed to identify T and B lymphocytes respectively, and correlated with SLP-2 staining.

Acknowledgments

We thank Drs. E. H. Ball, E. Cairns, T. L. Delovitch, H. M. McBride, B. Singh, and the members of the Madrenas laboratory for many insightful discussions, and Dr. A. Viola for the mtRFP expression plasmid. This work was supported by grants from the Canadian Institutes of Health Research (CIHR), the Kidney Foundation of Canada (Allison Knudsen Research Award), and the Multi-Organ Transplant Program of the London Health Sciences Centre (to J.M.)**,** NIH grant R01-AI43549 (to M.L.D.), NIH training grant T32-GM07308 (to S.V.), and FONACIT S1-2002000575 (to I.B.). M.G.K. is the recipient of a CIHR MD/PhD studentship, and J.M. holds a Canada Research Chair in Immunobiology.

References

1. Dustin, M.L. Stop and go traffic to tune T cell responses. *Immunity* **21**, 305-14 (2004).
2. Lee, K.H. et al. T cell receptor signaling precedes immunological synapse formation. *Science* **295**, 1539-42 (2002).
3. Lee, K.H. et al. The immunological synapse balances T cell receptor signaling and degradation. *Science* **302**, 1218-22 (2003).
4. Depoil, D. et al. Immunological synapses are versatile structures enabling selective T cell polarization. *Immunity* **22**, 185-94 (2005).

5. Saito, T. & Yokosuka, T. Immunological synapse and microclusters: the site for recognition and activation of T cells. *Curr Opin Immunol* **18**, 305-13 (2006).

6. Cullinan, P., Sperling, A.I. & Burkhardt, J.K. The distal pole complex: a novel membrane domain distal to the immunological synapse. *Immunol Rev* **189**, 111-22 (2002).

7. Arp, J. et al. Regulation of T-cell activation by phosphodiesterase 4B2 requires its dynamic redistribution during immunological synapse formation. *Mol Cell Biol* **23**, 8042-57 (2003).

8. Gascoigne, N.R. & Zal, T. Molecular interactions at the T cell-antigen-presenting cell interface. *Curr Opin Immunol* **16**, 114-9 (2004).

9. Varma, R., Campi, G., Yokosuka, T., Saito, T. & Dustin, M.L. T cell receptor-proximal signals are sustained in peripheral microclusters and terminated in the central supramolecular activation cluster. *Immunity* **25**, 117-27 (2006).

10. Mossman, K.D., Campi, G., Groves, J.T. & Dustin, M.L. Altered TCR signaling from geometrically repatterned immunological synapses. *Science* **310**, 1191-1193 (2005).

11. Rodgers, W., Farris, D. & Mishra, S. Merging complexes: properties of membrane raft assembly during lymphocyte signaling. *Trends Immunol* **26**, 97-103 (2005).

12. Huang, Y. & Burkhardt, J.K. T-cell-receptor-dependent actin regulatory mechanisms. *J Cell Sci* **120**, 723-30 (2007).

13. Billadeau, D.D., Nolz, J.C. & Gomez, T.S. Regulation of T-cell activation by the cytoskeleton. *Nat Rev Immunol* **7**, 131-43 (2007).

14. Quintana, A. et al. T cell activation requires mitochondrial translocation to the immunological synapse. *Proc Natl Acad Sci U S A* **104**, 14418-23 (2007).

15. Campello, S. et al. Orchestration of lymphocyte chemotaxis by mitochondrial dynamics. *J Exp Med* **203**, 2879-86 (2006).

16. Sprenger, R.R. et al. Comparative proteomics of human endothelial cell caveolae and rafts using two-dimensional gel electrophoresis and mass spectrometry. *Electrophoresis* **25**, 156-72 (2004).

17. Dowling, P. et al. Proteomic analysis of isolated membrane fractions from superinvasive cancer cells. *Biochim Biophys Acta* (2006).

18. Wang, Y. & Morrow, J.S. Identification and characterization of human SLP-2, a novel homologue of stomatin (band 7.2b) present in erythrocytes and other tissues. *J Biol Chem* **275**, 8062-71 (2000).

19. Owczarek, C.M. et al. A novel member of the STOMATIN/EPB72/mec-2 family, stomatin-like 2 (STOML2), is ubiquitously expressed and localizes to HSA chromosome 9p13.1. *Cytogenet Cell Genet* **92**, 196-203 (2001).

20. Seidel, G. & Prohaska, R. Molecular cloning of hSLP-1, a novel human brain-specific member of the band 7/MEC-2 family similar to Caenorhabditis elegans UNC-24. *Gene* **225**, 23-9 (1998).

21. Hiller, N.L., Akompong, T., Morrow, J.S., Holder, A.A. & Haldar, K. Identification of a stomatin orthologue in vacuoles induced in human erythrocytes by malaria parasites. A role for microbial raft proteins in apicomplexan vacuole biogenesis. *J Biol Chem* **278**, 48413-21 (2003).

22. Green, J.B. et al. Eukaryotic and prokaryotic stomatins: the proteolytic link. *Blood Cells Mol Dis* **32**, 411-22 (2004).

23. Tavernarakis, N., Driscoll, M. & Kyrpides, N.C. The SPFH domain: implicated in regulating targeted protein turnover in stomatins and other membrane-associated proteins. *Trends Biochem Sci* **24**, 425-7 (1999).

24. Morrow, I.C. & Parton, R.G. Flotillins and the PHB Domain Protein Family: Rafts, Worms and Anaesthetics. *Traffic* **6**, 725-40 (2005).

25. Hajek, P., Chomyn, A. & Attardi, G. Identification of a novel mitochondrial complex containing mitofusin 2 and stomatin-like protein 2. *J Biol Chem* **282**, 5670-5681 (2007).

26. Salzer, U. & Prohaska, R. Stomatin, flotillin-1, and flotillin-2 are major integral proteins of erythrocyte lipid rafts. *Blood* **97**, 1141-3 (2001).

27. Stewart, G.W. et al. Isolation of cDNA coding for an ubiquitous membrane protein deficient in high Na+, low K+ stomatocytic erythrocytes. *Blood* **79**, 1593-601 (1992).

28. Stewart, G.W., Argent, A.C. & Dash, B.C. Stomatin: a putative cation transport regulator in the red cell membrane. *Biochim Biophys Acta* **1225**, 15-25 (1993).

29. Gallagher, P.G. & Forget, B.G. Structure, organization, and expression of the human band 7.2b gene, a candidate gene for hereditary hydrocytosis. *J Biol Chem* **270**, 26358-63 (1995).

30. Huber, T.B. et al. Inaugural Article: Podocin and MEC-2 bind cholesterol to regulate the activity of associated ion channels. *Proc Natl Acad Sci U S A* **103**, 17079-86 (2006).

31. Huang, M., Gu, G., Ferguson, E.L. & Chalfie, M. A stomatin-like protein necessary for mechanosensation in C. elegans. *Nature* **378**, 292-5 (1995).

32. Rajaram, S., Sedensky, M.M. & Morgan, P.G. Unc-1: a stomatin homologue controls sensitivity to volatile anesthetics in Caenorhabditis elegans. *Proc Natl Acad Sci U S A* **95**, 8761-6 (1998).

33. Chelur, D.S. et al. The mechanosensory protein MEC-6 is a subunit of the C. elegans touch-cell degenerin channel. *Nature* **420**, 669-73 (2002).

34. Goodman, M.B. et al. MEC-2 regulates C. elegans DEG/ENaC channels needed for mechanosensation. *Nature* **415**, 1039-42 (2002).

35. Zhang, Y. et al. Identification of genes expressed in C. elegans touch receptor neurons. *Nature* **418**, 331-5 (2002).

36. Zhang, S. et al. MEC-2 is recruited to the putative mechanosensory complex in C. elegans touch receptor neurons through its stomatin-like domain. *Curr Biol* **14**, 1888-96 (2004).

37. Wetzel, C. et al. A stomatin-domain protein essential for touch sensation in the mouse. *Nature* (2006).

38. Allenspach, E.J. et al. ERM-dependent movement of CD43 defines a novel protein complex distal to the immunological synapse. *Immunity* **15**, 739-50 (2001).

39. Yokosuka, T. et al. Newly generated T cell receptor microclusters initiate and sustain T cell activation by recruitment of Zap70 and SLP-76. *Nat Immunol* (2005).

40. Iwashima, M., Irving, B.A., van Oers, N.S., Chan, A.C. & Weiss, A. Sequential interactions of the TCR with two distinct cytoplasmic tyrosine kinases. *Science* **263**, 1136-9 (1994).

41. Jones, N. et al. Nck adaptor proteins link nephrin to the actin cytoskeleton of kidney podocytes. *Nature* **440**, 818-23 (2006).

42. Da Cruz, S. et al. Proteomic analysis of the mouse liver mitochondrial inner membrane. *J Biol Chem* **278**, 41566-71 (2003).

43. Mootha, V.K. et al. Integrated analysis of protein composition, tissue diversity, and gene regulation in mouse mitochondria. *Cell* **115**, 629-40 (2003).

44. Schmitt, S. et al. Proteome analysis of mitochondrial outer membrane from Neurospora crassa. *Proteomics* **6**, 72-80 (2006).

45. Bathori, G. et al. Porin is present in the plasma membrane where it is concentrated in caveolae and caveolae-related domains. *J Biol Chem* **274**, 29607-12 (1999).

46. Rajendran, L. et al. Asymmetric localization of flotillins/reggies in preassembled platforms confers inherent polarity to hematopoietic cells. *Proc Natl Acad Sci U S A* **100**, 8241-6 (2003).

47. Liu, J., Deyoung, S.M., Zhang, M., Dold, L.H. & Saltiel, A.R. The stomatin/prohibitin/flotillin/HflK/C domain of flotillin-1 contains distinct sequences that direct plasma membrane localization and protein interactions in 3T3-L1 adipocytes. *J Biol Chem* **280**, 16125-34 (2005).

48. Rajalingam, K. et al. Prohibitin is required for Ras-induced Raf-MEK-ERK activation and epithelial cell migration. *Nat Cell Biol* **7**, 837-43 (2005).

49. Slaughter, N. et al. The flotillins are integral membrane proteins in lipid rafts that contain TCR-associated signaling components: implications for T-cell activation. *Clin Immunol* **108**, 138-51 (2003).

50. Stuermer, C.A. et al. PrPc capping in T cells promotes its association with the lipid raft proteins reggie-1 and reggie-2 and leads to signal transduction. *Faseb J* **18**, 1731-3 (2004).

51. Langhorst, M.F., Reuter, A. & Stuermer, C.A. Scaffolding microdomains and beyond: the function of reggie/flotillin proteins. *Cell Mol Life Sci* (2005).

52. McBride, H.M., Neuspiel, M. & Wasiak, S. Mitochondria: more than just a powerhouse. *Curr Biol* **16**, R551-60 (2006).

53. Lanzavecchia, A. & Sallusto, F. From synapses to immunological memory: the role of sustained T cell stimulation. *Curr Opin Immunol* **12**, 92-8 (2000).

54. Gett, A.V., Sallusto, F., Lanzavecchia, A. & Geginat, J. T cell fitness determined by signal strength. *Nat Immunol* **4**, 355-60 (2003).

55. Baroja, M.L. et al. The inhibitory function of CTLA-4 does not require its tyrosine phosphorylation. *J Immunol* **164**, 49-55 (2000).

56. Darlington, P.J. et al. Surface cytotoxic T lymphocyte-associated antigen 4 partitions within lipid rafts and relocates to the immunological synapse under conditions of inhibition of T cell activation. *J Exp Med* **195**, 1337-47 (2002).

TABLES

Table 1: Segregation of mitochondrial SLP2-gfp from the cSMAC in the mature IS, by wide field fluorescence microscopy

Segregation	No Segregation
25/29 (86.2%)	4/29 (13.8%)

Only cells forming IRM contacts for 3 or more data points were considered. Images of each field were taken at 2-3 minute intervals. Data is representative of 3 experiments.

Table 2: Percentage of Jurkat T cells on supported planar bilayers organizing SLP2-gfp close to pSMACs at the contact interface by wide field fluorescence microscopy

	Peripheral ring	No peripheral ring
10 μg/mL OKT3 + 300 mol/μm^2 ICAM-1	29[1]	8
300 mol/μm^2 ICAM-1 only	0	29

[1] $p < 0.0001$ vs. ICAM-1 only

FIGURE LEGENDS

Figure 1.- Expression of SLP-2 in the human immune system and its up-regulation upon lymphocyte activation. A) Commercially available human whole cell lysates from the indicated organs were sequentially immunoblotted for SLP-2 and GAPDH. Equal loading of protein per lane was further confirmed by spectroscopy. Results are representative of four independent experiments. B) Lymph node samples from non-specific B cell adenitis (top row) or T cell adenitis (middle row), and normal thymus (bottom rows) were stained for SLP-2 using a C-terminus specific rabbit anti-human SLP-2 antisera or with appropriate controls ($CD20^{bright}$ for B cells, TdT for developing thymocytes), and biotinylated horse anti-rabbit secondary antibody and avidin (Vector Labs, Burlingame CA). High levels of SLP-2 expression were detected in the germinal centres (B cell area) of lymph nodes of non-specific B cell adenitis, in the paracortical (T cell) area of non-specific T cell adenitis, and in the cortex of the thymus. Much lower expression of SLP-2 was seen in cells outside these areas. The profile of intracellular localization of SLP-2 was predominantly associated to the periphery of the cell and some aggregates in the central area of the cytoplasm. C) Human peripheral blood T cells were stimulated with syngeneic APC and SEE for 36 hours. Cell lysates were prepared and immunoblotted for SLP-2 and β-actin (as a loading control). Results are representative of three independent experiments. D) Human tonsil cells were fractionated through Percoll gradient and lysates from the four fractions were immunoblotted for SLP-2 and β-actin. B cell markers for naïve and activated memory B cells were used to determine the percentage of naïve and activated memory B cells in each fraction (shown in the table). Results are representative of two independent experiments.

Figure 2.- Localization of SLP-2 in T cells during activation. A) Intracellular and membrane-associated distribution of SLP-2-gfp in resting Jurkat cells. Stable, doxycycline-inducible, SLP-2-gfp-transfected E6.1 Jurkat T cells were examined by confocal microscopy. A low magnification of the field is shown to document that the high magnification pictures are representative of the T cell population. B) SLP-2 polarizes to the immunological synapse during activation of T cells. Stable SLP-2-gfp-transfected E6.1 Jurkat T cells were stimulated with APC and SEE, and examined under confocal microscope for the formation of synapses (identified as CD3 red clusters at the interface between T cell and APC). Images are representative of at least 50 putative immunological synapses. Concomitant studies done with control transfected T cells demonstrated that expression of SLP-2-gfp did not interfere with immunological synapse formation. Location of SLP-2-gfp as predominantly proximal to the IS, predominantly distal to the IS, or diffuse was quantified at 0 and 30 minutes of stimulation. C) SLP-2 redistributes to the periphery of the IS during T cell activation. Videomicroscopy capture of SLP-2-gfp during IS formation. The figures shown here were obtained at the indicated time periods. The video is available as supplementary data.

Figure 3.- Redistribution of plasma membrane-associated SLP-2 by TIRF (A) and mitochondrial membrane-associated SLP-2 (B and C) during immunological synapse formation. A) Membrane-associated SLP-2 segregates from TCR microclusters at early and late timepoints. Jurkat T cells stably expressing SLP2-gfp were treated with doxycycline 12 hrs prior to imaging, then incubated on bilayers containing ICAM1-cy5 and anti-human CD3 (OKT3) and imaged for 30 min. IRM and TCR images were obtained by wide-field fluorescence microscopy. SLP2-gfp was imaged using total internal reflection fluorescence microscopy

(TIRFM). Images were exposed for no longer than 900 ms with no greater than 15 μW of laser power. B) The intracellular SLP-2 pool organize into the periphery of the immunological synapse. Jurkat T cells stably transfected with SLP-2-gfp were incubated on bilayers containing ICAM-1 and anti-human CD3 (OKT3) and then imaged at 3 min and 30 min. Images shown were obtained by wide field fluorescence microscopy. The bright field images show the cells being imaged, the IRM images show contact with the bilayer as dark areas, and the TCR, ICAM-1 and SLP-2-gfp fluorescence channels are shown in gray scale and two red-green merges (green is always SLP-2). The dotted lines in the ICAM-1 pictures represent, from the periphery to the centre of the picture, the outer boundaries of the distal SMAC, of the pSMAC, and of the cSMAC. Images are representative 3 separate experiments. The video is available as supplementary data. C) The intracellular SLP-2 pool imaged by wide field localizes to the mitochondria of Jurkat T cells. Jurkat T Cells stably expressing SLP2-gfp were electroporated with the mitochondria-labeling mtRFP plasmid 12 hours before imaging. They were then incubated on bilayers containing ICAM-1 and anti-human CD3 (OKT3) and imaged at the indicated times. Images were obtained by wide-field fluorescence microscopy, and are representative of three separate experiments. The dotted lines in the ICAM-1 pictures represent, from the periphery to the centre of the picture, the outer boundaries of the distal SMAC, of the pSMAC, and of the cSMAC.

Figure 4.- Stable redistribution of SLP-2 during T cell activation and to membrane lipid rafts. Stable distribution of SLP-2 during T cell stimulation. Recovery from photobleaching in resting and activated stable SLP-2-gfp transfected T cells was measured during a 400 second window. Top graph illustrates recovery in resting T cells and bottom graph represents the profile

of recovery in activated T cells. Results are presented as mean ± S.D. of three different FRAP experiments. The video is available as supplementary data.

Figure 5.- Association of SLP-2 with components of the TCR signalosome and peripheral cytoskeleton during T cell activation. Jurkat T cells were stimulated with LG2 (as APC) and SEE for the indicated time. A) and C) SLP2 or pre-immune serum immunoprecipitates (lane 'C') (ip) with cross-linked antibody were sequentially immunoblotted for the indicated molecules and reblotted for SLP-2. B) LFA-1 immunoprecipitates were sequentially blotted for LFA-1 and for SLP-2. The amount of SLP-2 normalized to the amount of LFA was determined by densitometry. D) Inhibition of actin polymerization disrupts the association between SLP-2 and β-actin. E6.1 Jurkat T cells pretreated with cytochalasin D (10 μM) for 30 minutes were stimulated with APC and SEE for the indicated times. Whole cell lysates were prepared and used for immunoprecipitation of SLP-2 and immunoblotted for β-actin. Supernatants from 24 hour cultures of these T cells with APC and SEE were used to measure IL-2 production. Blots in these figure are representative of at least 4 separate experiments.

Figure 6.- Modulation of SLP-2 expression regulates T cell activation. A) Formation of immunological synapses by SLP-2-deficient (SLP-2 siRNA group) Jurkat T cells stimulated with APC and SEE for 30 min. IS were defined as clusters of CD3 in the T:APC interface. IS formation was quantified in the T:APC cultures for SLP-2 –deficient T cells (SLP-2 siRNA) and control groups, on three groups of 30 cell doublets each (**: $p<0.01$). An example of synapse-forming, SLP-2 siRNA-treated T cell is shown in #1 while #2 shows an example of a SLP-2 siRNA treated T cells failing to form a synapse. B) Jurkat T cells were nucleofected with

siRNA for SLP-2 or control siRNA and used for stimulation with APC and SEE for the indicated times. Cell lysates were prepared and immunoblotted for dually phosphorylated, active ERK-1/-2 and total ERK-1/-2. Signals for activated ERK-1/-2 and total ERK were quantified for each group at the indicated time points for three independent experiments and plotted as normalized densitometric units for activated ERK-1/-2. *: $p<0.05$, **: $p<0.01$.

Figure 7.- Modulation of SLP-2 expression regulates T cell activation. A) SLP-2 over-expression in Jurkat T cells was induced in stable transfectants for an inducible SLP-2-gfp cDNA with doxycycline. Down-regulation of SLP-2 levels in Jurkat T cells was done by siRNA. The response of these cells to APC and SEE was measured by IL-2 production. Expression of SLP-2-gfp was confirmed by FACS and knockdown of SLP-2 after siRNA was confirmed by Western blotting. B) Peripheral blood lymphocytes from a normal volunteer were isolated and used as resting cells, or after three days of *ex vivo* activation with PMA and ionomycin and 48hr of resting. Cells were nucleofected with SLP-2 siRNA or gfp control and used 24 hours later for stimulation with autologous APC and SEE. IL-2 production after 24 hours was assessed by ELISA. Additional control of cells nucleofected without any DNA was used to rule out non-specific effect of nucleofection. Inlet figure shows Western blot for SLP-2 to confirm knockdown of SLP-2, and β-actin as a loading control in the two groups tested. Similar results were obtained in 4 separate experiments. ***: $p<0.001$.

SUPPLEMENTAL FIGURE LEGENDS

Supplemental figure 1.- SLP-2 expression in human peripheral blood mononuclear cells (PBMC) of a healthy volunteer. Peripheral blood cells from an individual in whom low levels of expression of SLP-2 in PBMC were detected under resting conditions was used in this experiment to document expression of SLP-2 in different subsets of PBMC. T: T cells; B: B cells; M: monocytes.

Supplemental figure 1.- SLP-2 expression in human peripheral blood mononuclear cells (PBMC) of a healthy volunteer. Peripheral blood cells from an individual in whom low levels of expression of SLP-2 in PBMC were detected under resting conditions was used in this experiment to document expression of SLP-2 in different subsets of PBMC. T: T cells; B: B cells; M: monocytes.

Supplemental figure 3.- Compartmentalization of SLP-2 in human T cells. Lysates from intracellular compartments prepared from peripheral blood T cells by sequential solubilization and centrifugation were immunoblotted for SLP-2 and controls for each intracellular compartment.

Supplemental figure 4.- Increased relocation of SLP-2 into lipid rafts with TCR-dependent T cell activation. E6.1 Jurkat T cells were activated with APC and SEE for the indicated times. Membrane lipid rafts and the detergent-soluble fraction were isolated by sucrose gradient centrifugation and immunoblotted for SLP-2, ERK-1/-2 (as control for the quality of the detergent-soluble fraction), and GM-1 (as a control for the quality of lipid rafts). The SLP-2

signal (mean ± S.D.) for lipid raft fractions from T cells activated for different times in three experiments was quantified by densitometry.

Supplemental figure 5.- Interaction between SLP-2 and the CD3e chain of the TCR complex on Jurkat T cells. T cells ($27x10^6$ cells/group) were used to immunoprecipitate SLP-2 or CD3e using cross-linked antibodies. Immunoprecipitates (ip) and control whole T cell lysates (from $1.5x10^6$ cells) were blotted for either SLP-2 or CD3e and signals quantified by densitometry. The amount of SLP-2 associated to CD3e represented 0.09% of total SLP-2 levels in the cell.

Supplemental figure 6.- Interaction between SLP-2 and cell surface receptors on Jurkat T cells. Jurkat T cells stably transfected for wild type SLP-2-gfp or for a SLP-2-gfp lacking the N terminus (aa 1 to 77) were biotinylated. Next, biotinylated receptors were immunoprecipitated with an antibody against biotin or with beads alone as control, and immunoblotted for SLP-2. Whole cell lysates from the transfectants were used to control for expression of the transgenes. Only SLP-2-gfp and endogenous SLP-2 interacts with surface receptors, while the mutant SLP-2 without the membrane targeting N terminus does not. Note that Jurkat T cells express endogenous SLP-2 in addition to the transfected form.

Supplemental figure 7.- Down-regulation of SLP-2 does not affect IL-2 response to mitogenic stimulation with PMA and ionomycin. Peripheral blood lymphocytes from the experiment shown in figure 7B were used after three days of *ex vivo* activation and 48hr of resting. Cells were nucleofected with SLP-2 siRNA and used 24 hours later for stimulation with

PMA and ionomycin. IL-2 production after 24 hours was assessed by ELISA. Cells nucleofected without any DNA or with non-sense siRNA were used as controls. The effect of SLP-2 siRNA on SLP-2 levels are shown in right panel of figure 7B.

SUPPLEMENTAL VIDEO LEGENDS

Supplemental video 1.- Localization of SLP-2 during IS formation. Antigen presenting cells (APCs) were incubated overnight with SEE (1 μg/ml), washed, resuspended in medium, and incubated on polylysine-coated glass bottom microwell dishes for 10 minutes to allow cells to adhere. SLP-2-gfp-expressing Jurkat T cells were added to the APCs preincubated with SEE on the polylysine-coated microwell dishes. Once T:APC doublet was identified, images were acquired every 30 seconds for 60 minutes. The majority of SLP-2-gfp localized proximal to the synapse and distributed evenly in early stages, and as the IS matures SLP-2-gfp moved to periphery of the synapse.

Supplemental videos 2A and 2B.- SLP2 organizes into a peripheral ring in Jurkat Cells on planar bilayers containing anti-human CD3 + ICAM-1 but not on bilayers containing ICAM-1 alone. Jurkat T cells were incubated on bilayers containing ICAM-1 and anti-human CD3 (OKT3) (A) or ICAM-1 alone (B) and imaged by wide-field fluorescence microscopy from 1-40 minutes after the cells were applied.

Supplemental videos 3A and 3B.- Stability of SLP-2 clusters during T cell activation. Jurkat T cells stably expressing SLP-2-gfp were incubated on polylysine-coated glass bottom microwell dishes for 10 minutes to allow cells to adhere. Adherent Jurkat T cells were then stimulated with OKT3 (1 μg/ml) for 15 minutes. Non-stimulated (A) or stimulated (B) SLP-2-gfp expressing Jurkat T cells were then placed under confocal microscope. Forty images were acquired over a 375 seconds, with three images acquired before photobleaching. Area of cell indicated by arrow was photobleached using 100 % of laser power for 3 seconds and the movement of SLP-2-gfp

back into photobleached area was measured. Note that, in the stimulated T cell, it corresponds to an area with SLP-2-gfp clusters. Stimulated Jurkat T cells show little to no recovery of gfp signal in photobleached area, while non-stimulated cells show significant recovery of SLP-2-gfp in photobleached area within the examined time window.

Table 1: Segregation of mitochondrial SLP2-gfp from the cSMAC in the mature IS, by wide field fluorescence microscopy

Segregation	No Segregation
25/29 (86.2%)	4/29 (13.8%)

Only cells forming IRM contacts for 3 or more data points were considered. Images of each field were taken at 2-3 minute intervals. Data is representative of 3 experiments.

Table 2: Percentage of Jurkat T cells on supported planar bilayers organizing SLP2-gfp close to pSMACs at the contact interface by wide field fluorescence microscopy

	Peripheral ring	No peripheral ring
10 μg/mL OKT3 + 300 mol/μm^2 ICAM-1	29[1]	8
300 mol/μm^2 ICAM-1 only	0	29

[1] $p < 0.0001$ vs. ICAM-1 only

A

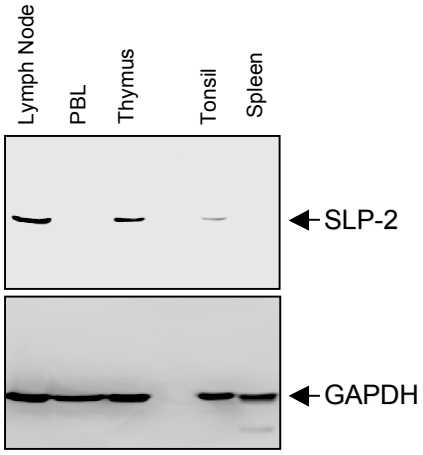

B

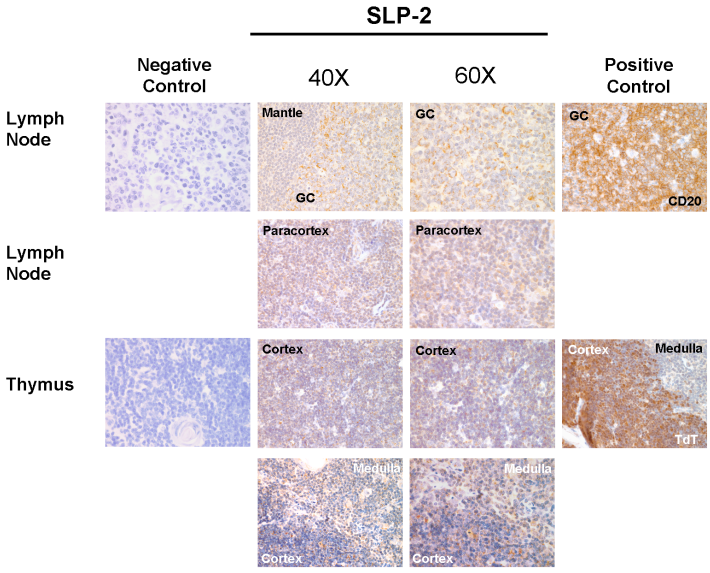

C

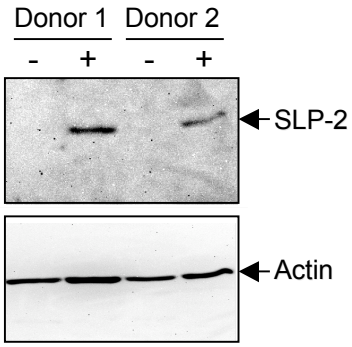

D

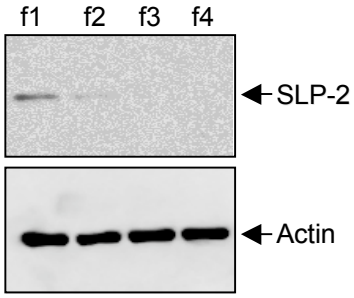

	Percent of human tonsil cells			
	f1	f2	f3	f4
$CD20^+/CD27^+/IgG^+$	24	19	12	3
$CD20^+/CD27^+/IgA^+$	36	25	15	5
$CD19^+/CD27^+/IgM^+$	13	8	5	3
$CD19^+/IgM^+/IgD^+$	8	17	45	60

Kirchhof et al: Figure 1

A

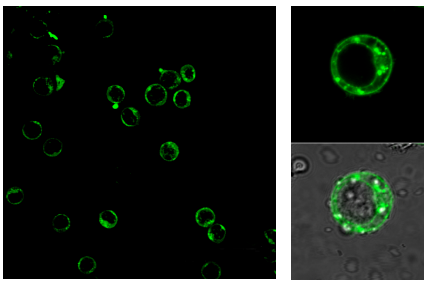

B

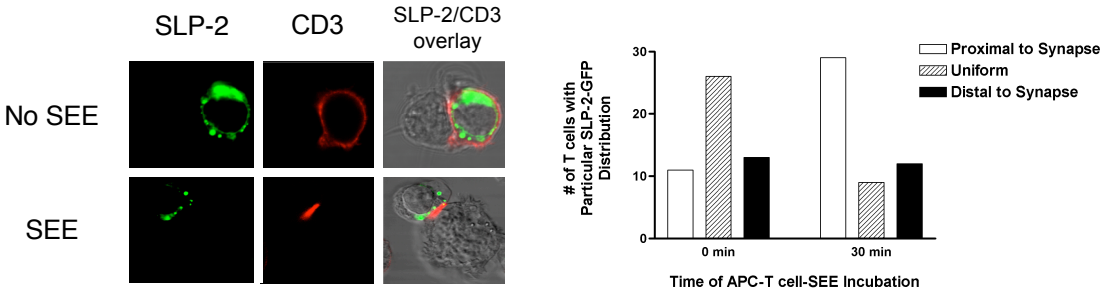

C

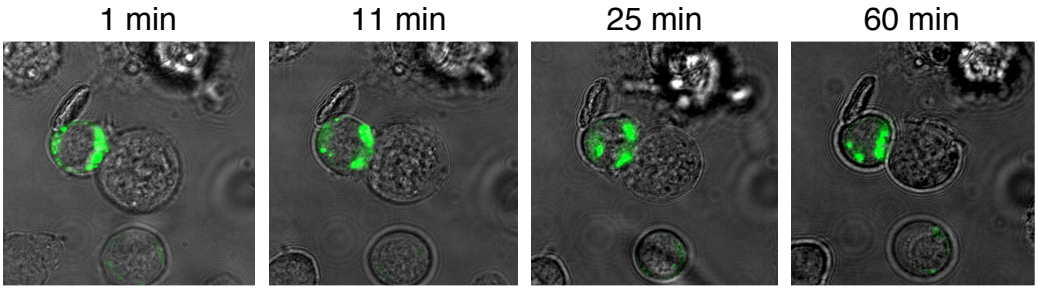

Kirchhof et al: Figure 2

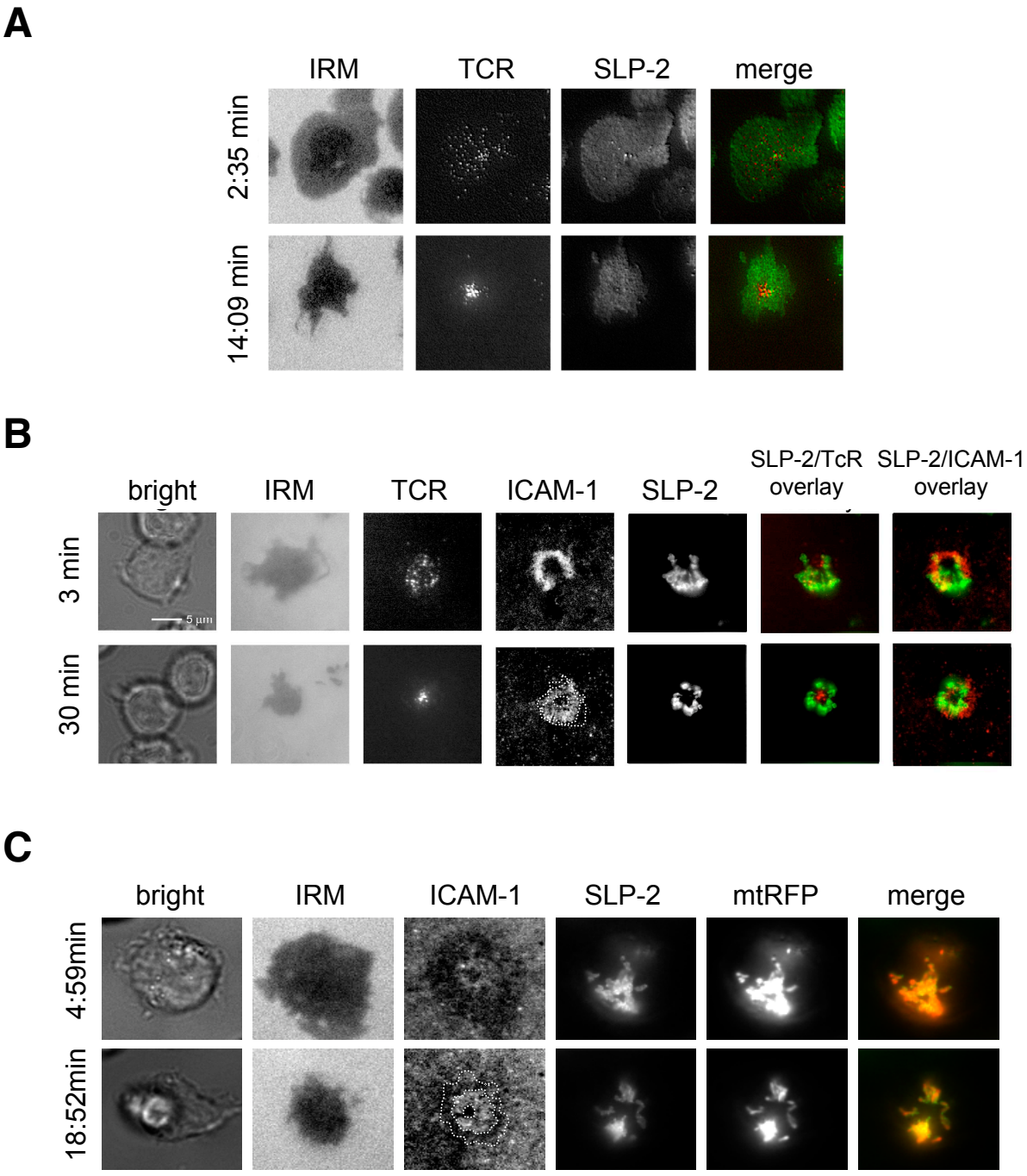

Kirchhof et al: Figure 3

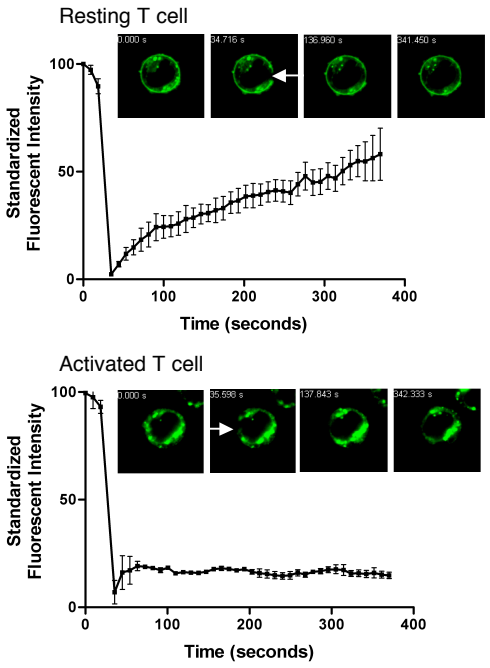

Kirchhof et al: Figure 4

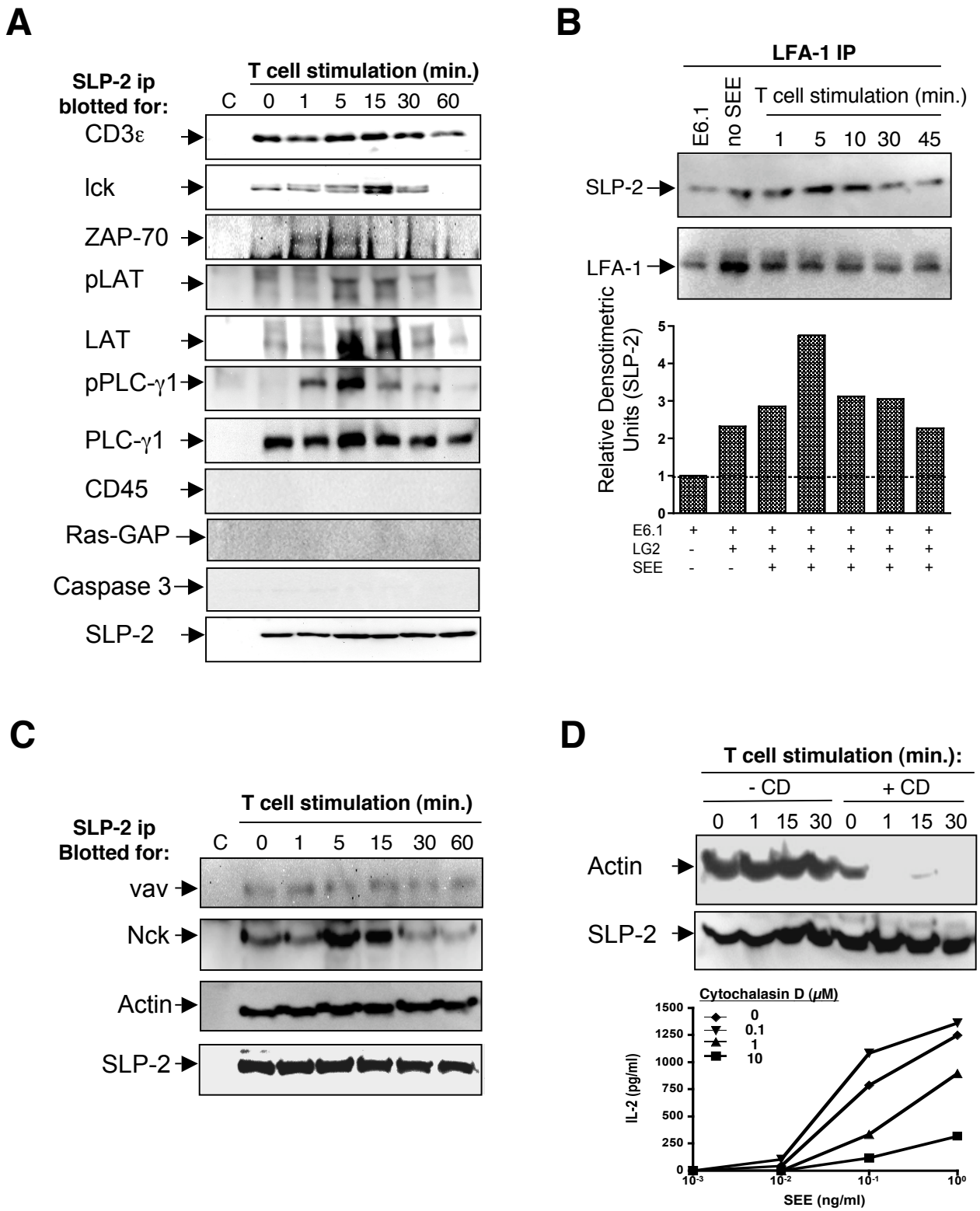

Kirchhof et al: Figure 5

A

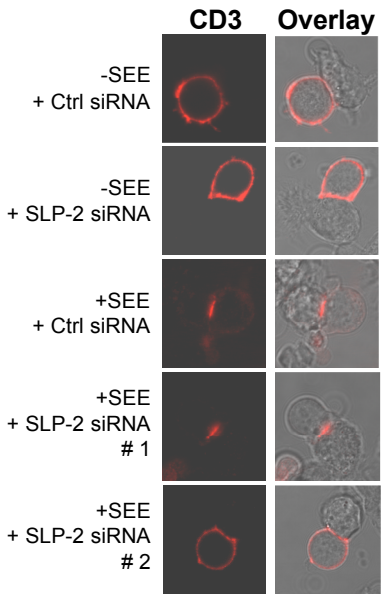

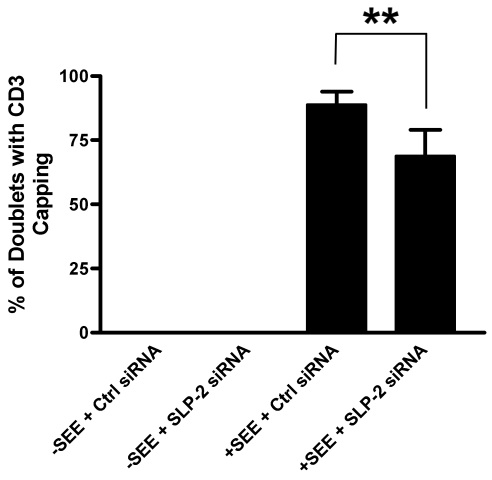

B

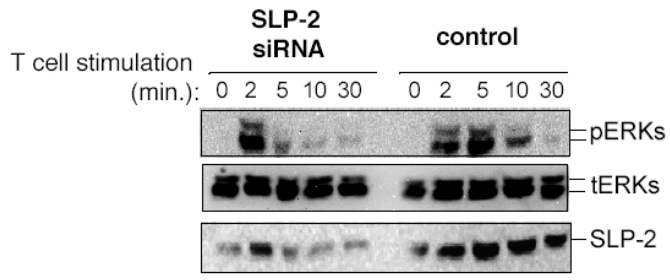

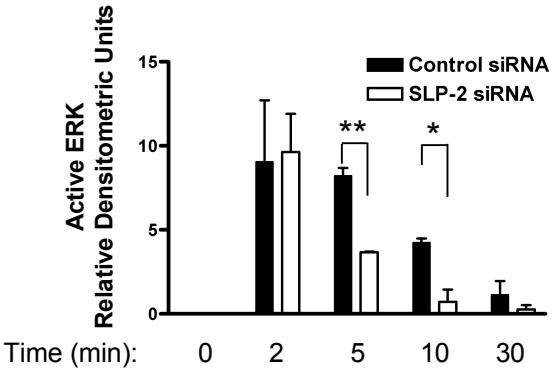

Kirchhof et al: Figure 6

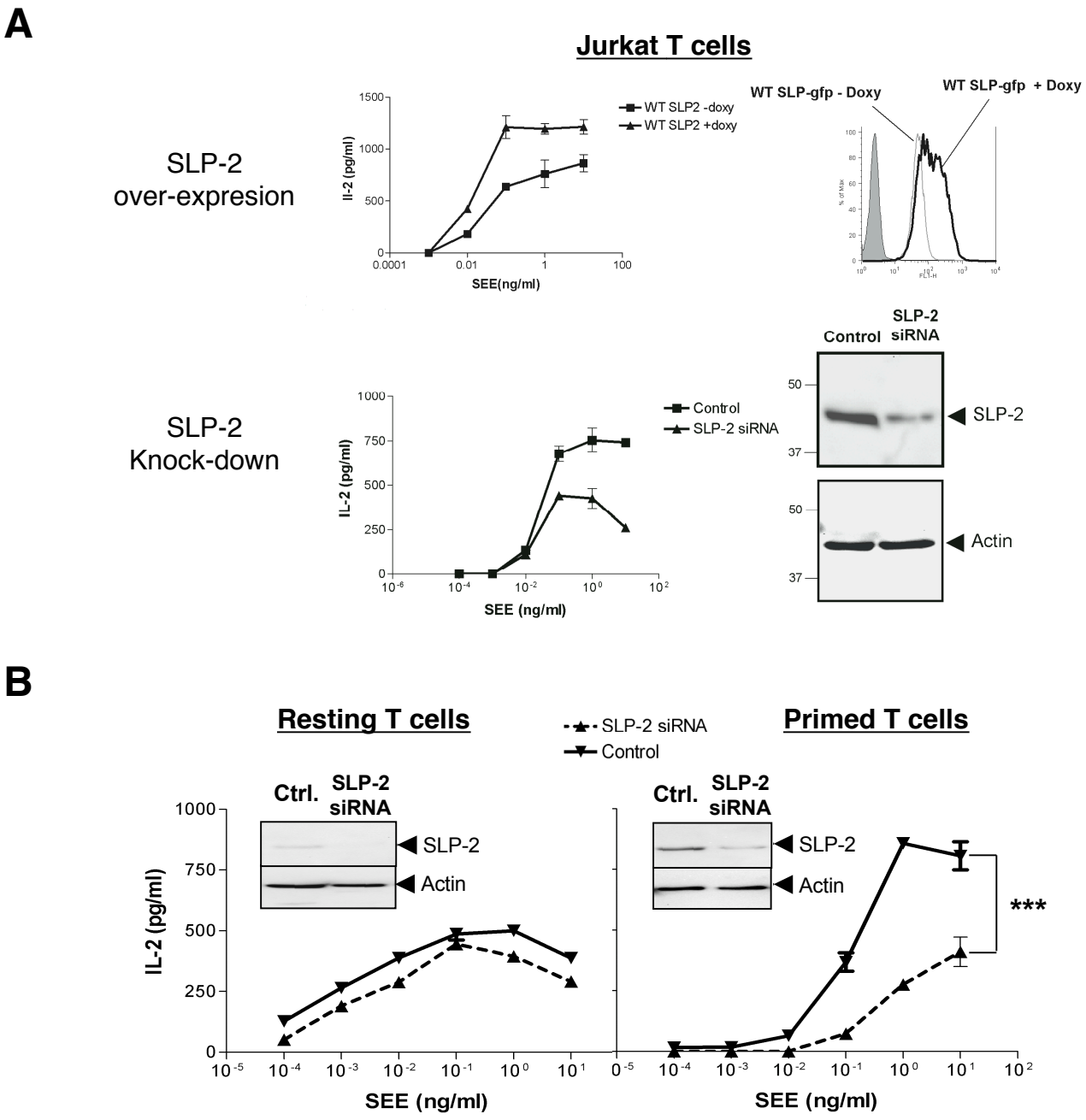

Kirchhof et al: Figure 7